

Biaxial strain tuned electronic structures and power factor in Janus Transition Metal Dichalcogenide monolayers

San-Dong Guo

Department of Physics, School of Sciences, China University of Mining and Technology, Xuzhou 221116, Jiangsu, China

Tuning physical properties of transition metal dichalcogenide (TMD) monolayers by strain engineering have most widely studied, and recently Janus TMD monolayer MoSSe has been synthesized. In this work, we systematically study biaxial strain dependence of electronic structures and transport properties of Janus TMD MXY (M = Mo or W, X/Y = S, Se, or Te) monolayer by using generalized gradient approximation (GGA) plus spin-orbit coupling (SOC). It is found that SOC has a noteworthy detrimental influence on power factor in p-type MoSSe, WSSe, n-type WTe, p-type MoSeTe and WSeTe, and has a negligible influence on one in n-type MoSSe, MoSTe, p-type WSTe and n-type MoSeTe. These can be understood by considering SOC effects on their valence and conduction bands. For all six monolayers, the energy band gap firstly increases, and then decreases, when strain changes from compressive one to tensile one. It is found that strain can tune strength of bands convergence of both valence and conduction bands by changing the numbers and relative position of valence band extrema (VBE) or conduction band extrema (CBE), which can produce very important effects on their electronic transport properties. By applying appropriate compressive or tensile strain, both n- or p-type Seebeck coefficient can be enhanced by strain-induced band convergence, and then the power factor can be improved. Our works further enrich studies on strain dependence of electronic structures and transport properties of new-style TMD monolayers, and motivate farther experimental works.

PACS numbers: 72.15.Jf, 71.20.-b, 71.70.Ej, 79.10.-n

Email:sandongyuwang@163.com

Keywords: Strain; Spin-orbit coupling; Power factor; Transition metal dichalcogenide monolayers

I. INTRODUCTION

Due to direct hot-electricity conversion without moving parts, thermoelectric materials have enormous potential to solve energy issues, and the efficiency of thermoelectric conversion can be measured by the dimensionless figure of merit^{1,2}, $ZT = S^2\sigma T/(\kappa_e + \kappa_L)$, in which S is the Seebeck coefficient, σ is electrical conductivity, T is absolute temperature, κ_e and κ_L are the electronic and lattice thermal conductivities, respectively. Based on the expression of ZT , an excellent efficiency of thermoelectric conversion requires high power factor ($S^2\sigma$) and low thermal conductivity ($\kappa = \kappa_e + \kappa_L$). However, the S and σ are oppositely proportional to the carrier concentration. Due to simultaneously increasing $S^2\sigma$ and decreasing κ , low-dimensional materials may have potential advantages in improving ZT ³⁻⁵.

Since the discovery of graphene⁶, two-dimensional (2D) materials have been attracting increasing attention, such as TMD, group-VA, group IV-VI and group-IV monolayers⁷⁻¹¹. The heat transport properties of these 2D materials have been widely studied, such as TMD, orthorhombic group IV-VI, group-VA, SnSe₂, ATeI (A=Sb or Bi) and TiS₂ monolayers¹²⁻¹⁹. In semiconducting TMD monolayers MX₂ (M=Zr, Hf, Mo, W or Pt; X=S, Se, or Te), the SOC is proved to be very important for electronic transport properties²⁰. Strain effects on the electronic structures and heat transport properties of TMD monolayers have been widely investigated both in theory and experiment. A semiconductor-to-metal transition can be observed by a small compressive strain (about 3%) in PtTe₂, compared with MoS₂ with very

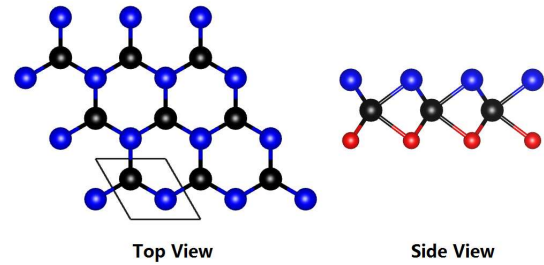


FIG. 1. (Color online) The schematic crystal structure of Janus MXY (M = Mo or W, X/Y = S, Se, or Te) monolayer. The black balls represent M atoms, and the red and blue balls for X/Y atoms.

large strain^{21,22}. For MoS₂, the significantly enhanced power factor can be observed in n(p)-type doping by compressive (tensile) strain at the critical strain of direct-indirect gap transition²³. It is found that tensile strain can improve thermoelectric properties of ZrS₂, PtSe₂ and PtTe₂ by enhancing $S^2\sigma$ and reducing κ_L ^{21,24,25}.

Recently, Janus monolayer MoSSe has been experimentally achieved by breaking the out-of-plane structural symmetry of MoS₂, replacing the top S atomic layer with Se atoms²⁶. It is found that Janus MoSSe monolayer can be used as a potential wide solar-spectrum water-splitting photocatalyst with a low carrier recombination rate²⁷. In monolayer and multilayer Janus TMD MXY (M = Mo or W, X/Y = S, Se, or Te), the strong piezoelectric effects have been observed by first-principles calculations²⁸. It is found that the carrier mobility in monolayer MoSSe is relatively low, but

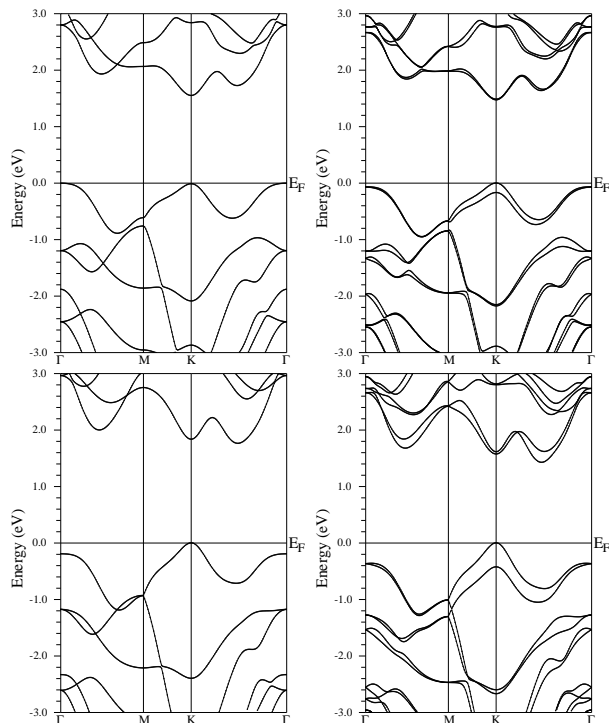


FIG. 2. The energy band structures of MoSSe (Top) and WSe (Bottom) using GGA (Left) and GGA+SOC (Right).

the bilayer or trilayer structures show a quite high electron/hole carrier mobility²⁹. Electronic and optical properties have been investigated in pristine Janus MoSSe and WSe monolayers, as well as their vertical and lateral heterostructures³⁰. It is found that the κ_L of MoSSe monolayer is higher than that of MoSe₂ monolayer, but is very lower than that of MoS₂ monolayer³¹. Calculated results show that ZrSSe monolayer predicted with the 1T phase has better n-type thermoelectric properties than monolayer ZrS₂³².

In this work, the biaxial strain dependence of electronic structures and transport properties of Janus TMD MXY (M = Mo or W, X/Y = S, Se, or Te) monolayers are studied by first-principles calculations and Boltzmann equation. It is very crucial for Janus TMD monolayers to include SOC for attaining reliable electronic structures and transport properties, which is similar with TMD monolayers^{20,21,23}. For all six Janus TMD monolayers, the energy band gap shows a nonmonotonic up-and-down behavior with increasing strain, while the spin-orbit splitting at *K* point monotonically increases. Calculated results show that strain can tune strength of bands convergence of valence (conduction) bands by changing the numbers and relative position of VBE (CBE), which can obviously affect their electronic transport properties. Both n- or p-type Seebeck coefficient can be enhanced by applying appropriate compressive or tensile strain, and then the power factor can be improved. Similar strain-improved power factor can also be found in TMD monolayers^{21,23-25}.

TABLE I. For MXY (M = Mo or W, X/Y = S, Se, or Te) monolayer, the lattice constants²⁸ a (Å); the calculated energy band gaps using GGA G (eV) and GGA+SOC G_{so} (eV); $G-G_{so}$ (eV); the spin-orbit splitting value Δ (eV) at *K* point in the valence bands around the Fermi level.

| Name | a | G | G_{so} | $G-G_{so}$ | Δ |
|--------|-------|------|----------|------------|----------|
| MoSSe | 3.252 | 1.55 | 1.47 | 0.08 | 0.168 |
| MoSTe | 3.327 | 1.17 | 1.14 | 0.03 | 0.181 |
| MoSeTe | 3.394 | 1.34 | 1.22 | 0.12 | 0.196 |
| WSSe | 3.220 | 1.76 | 1.43 | 0.33 | 0.426 |
| WSTe | 3.325 | 1.35 | 1.21 | 0.14 | 0.396 |
| WSeTe | 3.391 | 1.67 | 1.08 | 0.59 | 0.433 |

The rest of the paper is organized as follows. In the next section, we shall describe computational details about electronic structures and transport properties. In the third section, we shall present strain dependence of the electronic structures and transports properties of Janus TMD MXY (M = Mo or W, X/Y = S, Se, or Te) monolayers. Finally, we shall give our discussions and conclusion in the fourth section.

II. COMPUTATIONAL DETAIL

A full-potential linearized augmented-plane-waves method within the density functional theory (DFT)³³ is used to investigate strain dependence of electronic structures of MXY (M = Mo or W, X/Y = S, Se, or Te) monolayer, as implemented in the WIEN2k package³⁴. We employ the popular GGA of Perdew, Burke and Ernzerhof (GGA-PBE)³⁵ for the exchange-correlation potential, and the internal position parameters are optimized with a force standard of 2 mRy/a.u.. The SOC was included self-consistently³⁶⁻³⁹, which can produce important effects on both electronic structure and transport coefficients. To attain reliable results, we use 5000 k-points in the first Brillouin zone (BZ) for the self-consistent calculation, make harmonic expansion up to $l_{\max} = 10$ in each of the atomic spheres, and set $R_{\text{mt}} * k_{\max} = 8$. The self-consistent calculations are considered to be converged when the integration of the absolute charge-density difference between the input and output electron density is less than $0.0001|e|$ per formula unit, where e is the electron charge.

Based on calculated energy band structures, transport coefficients, such as Seebeck coefficient and electrical conductivity, are performed through solving Boltzmann transport equations within the constant scattering time approximation (CSTA) as implemented in BoltzTrap⁴⁰. To achieve the convergence results, the parameter LP-FAC is set to 40. The accurate transport coefficients need dense k-point meshes, and at least 2400 k-points is used in the irreducible BZ for the energy band calculation. It is noted that, for 2D material, the calculated

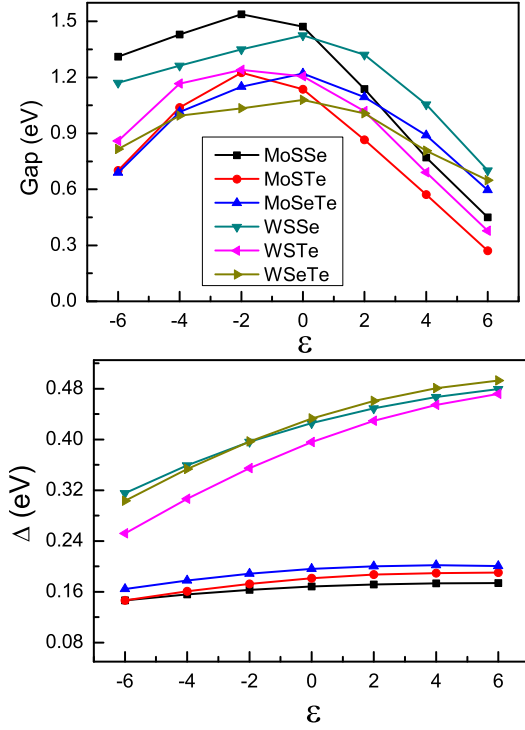


FIG. 3. (Color online) For MXY (M = Mo or W, X/Y = S, Se, or Te) monolayer, the energy band gap (Gap) and spin-orbit splitting value (Δ) at high symmetry K point as a function of ϵ by using GGA+SOC.

electrical conductivity depends on the length of unit cell along z direction⁴¹. They should be normalized by multiplying Lz/d , in which Lz is the length of unit cell along z direction, and d is the thickness of 2D material. It is well known that the d is not well defined like graphene. In this work, the $Lz=20$ Å is used as d .

III. MAIN CALCULATED RESULTS AND ANALYSIS

The structure of Janus MXY (M = Mo or W, X/Y = S, Se, or Te) monolayer (Figure 1) is similar to MX₂ monolayer with the 2H phase, which contains three atomic sublayers with M layer sandwiched between X and Y layers. Compared with MX₂, the Janus MXY monolayer lacks the reflection symmetry with respect to the central metal M atoms. With the sandwiched S-Mo-Se structure, Janus TMD monolayer MoSSe has been experimentally achieved by replacing the top S atomic layer in MoS₂ with Se atoms²⁶. To avoid spurious interaction between neighboring layers, the unit cell of Janus MXY monolayer, containing one M, one X and one Y atoms, is constructed with the vacuum region of more than 18 Å. The optimized lattice constants²⁸ for MXY are listed in Table I using GGA.

It has been proved that SOC can produce important effects on electronic structures for MX₂ (M=Zr, Hf, Mo,

W or Pt; X=S, Se, or Te), and further influences their thermoelectric properties^{20,21,23,25}. Due to similar crystal structure and element type between TMD and Janus TMD monolayers, the SOC is included for all calculations of Janus TMD monolayers. Figure 2 shows the calculated energy bands for monolayer MoSSe and WSe with GGA and GGA+SOC, and FIG.1 and FIG.2 in the Supporting Information (SI) show ones of monolayer MoSTe, WSTe, MoSeTe and WSeTe. For monolayer MoSSe, the indirect gap of 1.55 eV is calculated with valence band maximum (VBM) at Γ point and conduction band minimum (CBM) at K point using GGA. A second maxima appears at K point, which is 0.01 eV lower than VBM. When the SOC is considered, the VBM changes from Γ point to K point with a direct gap of 1.47 eV, and the energy difference between Γ and K is 0.07 eV. It is noted that these results sensitively depend on lattice constants. For WSSe, the CBM is along the Γ -K direction, and an indirect gap of 1.76 eV (1.43 eV) using GGA (GGA+SOC) is defined with the VBM at the Γ point. For MoSTe and WSTe, the CBM and VBM are located along the Γ -K direction and at Γ point. The MoSeTe and WSeTe have indirect gaps with the CBM and VBM along the Γ -K direction and at K point. The GGA gaps, GGA+SOC gaps and the differences between them are shown in Table I. It is found that the gaps with GGA+SOC are smaller than ones with GGA for all materials, which is caused by spin-orbit splitting. It is found that the Rashba spin-orbit splitting exists at Γ point of valence bands because of lacking the inversion symmetry. The gap difference between GGA and GGA+SOC can reflect the SOC influences on the conduction bands, and the larger gap decrease means the stronger SOC. The SOC effects on the valence bands near Fermi level can be described by spin-orbit splitting at the K point, which are summarized in Table I. It is clearly seen that WXY has larger spin-orbit splitting than MoXY.

Both in theory and in experiment, strain effects on the energy band structures and transport properties of TMD monolayers have been widely investigated^{21,23-25,42}. Here, biaxial strain effects on the electronic structures and electronic transport coefficients of MXY (M = Mo or W, X/Y = S, Se, or Te) monolayer are studied. To simulate biaxial strain, $\epsilon = (a - a_0)/a_0$ is defined, where a_0 is the unstrained lattice constant. $\epsilon < 0$ means compressive strain, while $\epsilon > 0$ implies tensile strain. Using GGA+SOC, the energy band gap and spin-orbit splitting value at K point in the valence bands around the Fermi level as a function of ϵ are plotted in Figure 3. For all materials, the energy band gap firstly increases, and then decreases, when ϵ changes from -6% to 6%. Similar strain dependence of energy band gap can also be found in TMD monolayers^{21,23-25}. As ϵ increases, the spin-orbit splitting at K point monotonically increases, and the change is 0.027–0.044 eV for MoXY and 0.164–0.220 eV for WXY, which means the spin-orbit splitting has stronger dependence on strain for WXY than MoXY. With increasing strain, the trend of spin-orbit splitting

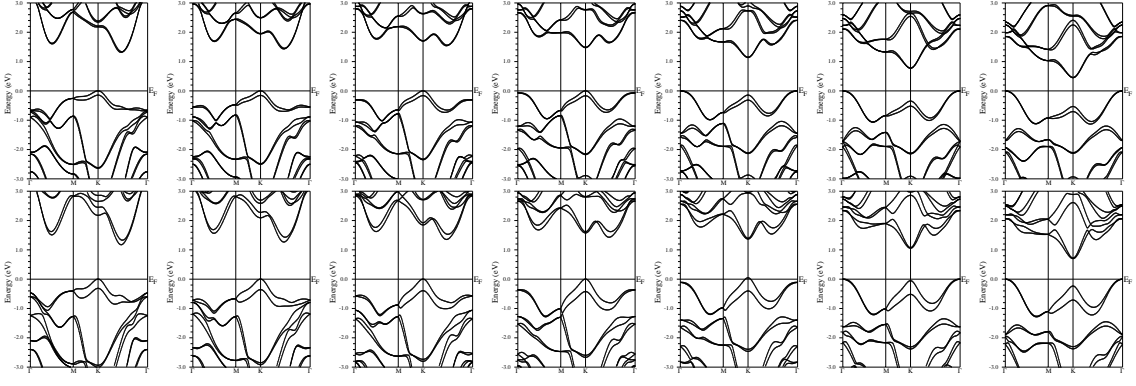


FIG. 4. The energy band structures of MoSSe (Top) and WSe (Bottom) with ε changing from -6% to 6% using GGA+SOC, and the strain increment for 2%.

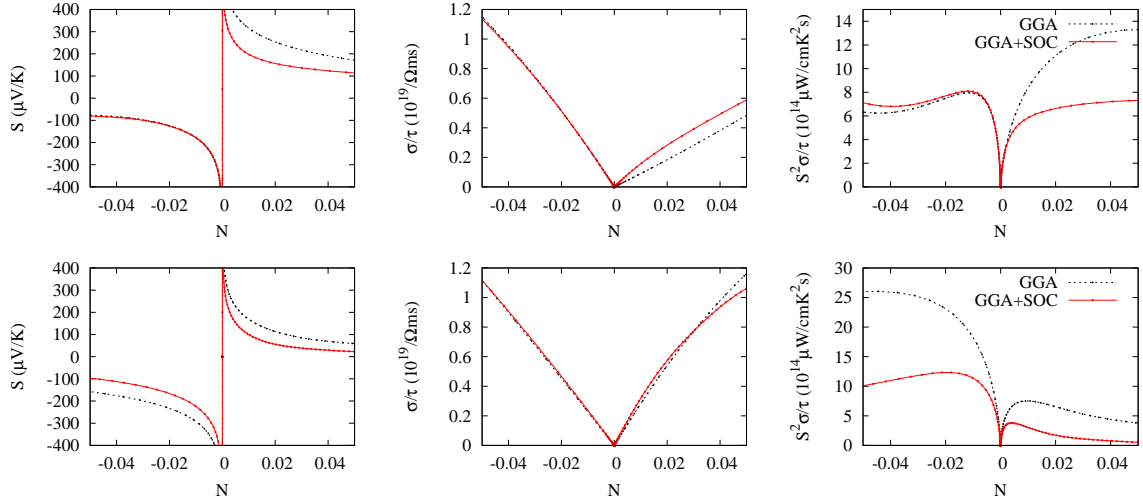


FIG. 5. (Color online) the room-temperature transport coefficients of MoSSe (Top) and WSe (Bottom) as a function of doping level (N) using GGA and GGA+SOC: Seebeck coefficient S , electrical conductivity with respect to scattering time σ/τ and power factor with respect to scattering time $S^2\sigma/\tau$.

is consistent with one of MoS₂²³, but is opposite to one of PtSe₂²⁵ or PtTe₂²¹.

For monolayer MoSSe and WSe, the related energy band structures with strain from -6% to 6% are also shown in Figure 4 using GGA+SOC, and FIG.3 and FIG.4 in the SI show ones of monolayer MoSTe, WSTe, MoSeTe and WSeTe. For all materials, there are some VBE and CBE around the Fermi level. It is found that strain can tune the numbers and relative position of VBE or CBE, which can produce very important influences on their electronic transport properties. The compressive strain can reduce the numbers of CBE from three to two, and tensile strain from three to one. Both compressive and tensile strain can change relative position of VBE. In a word, strain can tune strength of bands convergence of both conduction and valence bands. The similar phenomenon can also be observed in TMD monolayers^{21,23-25,42}.

The transport coefficients calculations are performed, based on CSTA Boltzmann theory within rigid band ap-

proach. The calculated electrical conductivity σ/τ depends on scattering time, while Seebeck coefficient S is independent of scattering time. By simply moving the position of Fermi level, the doping effects can be simulated. When the Fermi level is shifted into conduction (valence) bands, the n(p)-type doping is achieved with negative (positive) doping levels, giving the negative (positive) Seebeck coefficient. For monolayer MoSSe and WSe, at room temperature, the Seebeck coefficient S , electrical conductivity with respect to scattering time σ/τ and power factor with respect to scattering time $S^2\sigma/\tau$ as a function of doping level (N) using GGA and GGA+SOC are plotted in Figure 5, and FIG.6 in the SI show ones of monolayer MoSTe, WSTe, MoSeTe and WSeTe. For MoXY, a detrimental influence on p-type S can be induced by SOC, while a neglectful effect on S (absolute value) in n-type doping can be observed. The SOC can lift the valence band degeneracy near the K point, which reduces slope of density of states (DOS) of valence bands near the energy gap,

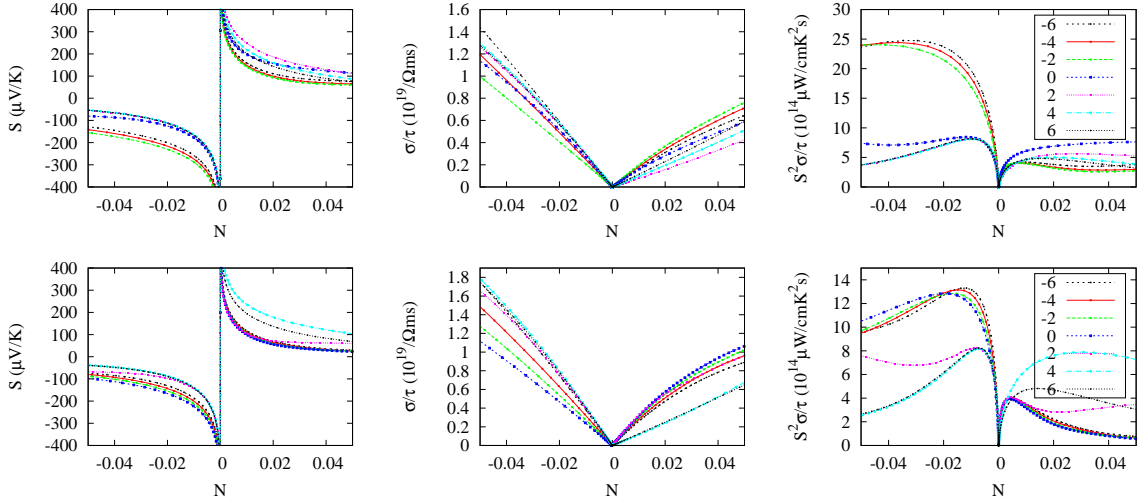


FIG. 6. (Color online) the room-temperature transport coefficients of MoSSe (Top) and WSe (Bottom) as a function of doping level (N) using GGA+SOC with ε changing from -6 to 6: Seebeck coefficient S , electrical conductivity with respect to scattering time σ/τ and power factor with respect to scattering time $S^2\sigma/\tau$.

giving rise to reduced Seebeck coefficient. However, the weak SOC effects on conduction bands near the Fermi level are observed, leading to a neglectful effect on n-type S . For WXY, a reduced influence on both n- and p-type S can be observed at the presence of SOC, which can be explained by SOC-induced spin-orbit splitting of both conduction and valence bands, reducing slope of DOS near the energy gap. In n-type doping, the power factor of WXY with GGA+SOC is smaller than one using GGA. For Mo/WSSe and Mo/WSeTe, p-type power with GGA+SOC is lower than one with GGA. These can be understood by SOC effects on S and σ/τ . It is noted that these results depend on the lattice constants. When the SOC is considered, the strength of bands convergence is enhanced, and the S would be improved, producing enhanced power factor, which has been observed in TMD monolayer WX_2 ($X=S, Se$ and Te)²⁰.

At 300 K, the biaxial strain dependence of S , σ/τ and $S^2\sigma/\tau$ of monolayer MoSSe and WSe are shown in Figure 6 using GGA+SOC, and FIG.7 and FIG.8 in the SI show ones of monolayer MoSTe, WSTe, MoSeTe and WSeTe. The complex strain dependence of transport coefficients are observed, which is because their energy band structures are sensitively dependent on strain. Strain-enhanced S can be understood by strain-driven accidental degeneracies, namely bands convergence. For example MoSSe, in considered n-type doping range, the largest S can be observed with -2% strain due to the near degeneracy among CBE along K- Γ , along Γ -M and at K point. In fact, the MoSSe with -6% and -4% strain have similar S with one with -2% due to the bands convergence of CBE along K- Γ and Γ -M, leading to very large n-type power factor. In p-type doping of WSe, S reaches the largest values with 4% strain due to the energy levels of K and Γ points being more close, leading to largest p-type power factor. It is found that the σ/τ and S show

usually opposite strain dependence. For MoSSe, WSe, MoSTe and MoSeTe, strain-enhanced n-type power factor is larger than p-type one, while it is opposite for WSTe and WSeTe. An upper limit of ZT , neglecting κ_L , can be defined as $ZT_e = S^2\sigma T/\kappa_e$. The κ_e relates to σ via the Wiedemann-Franz law: $\kappa_e = L\sigma T$, and then $ZT_e = S^2/L$, where L is the Lorenz number. Therefore, the power factor is improved by enhanced S induced by strain, which is beneficial to better thermoelectric properties. Strain-improved power factor can also be observed in TMD monolayers^{21,23-25,42}.

IV. DISCUSSIONS AND CONCLUSION

For TMD monolayers, the SOC produces a remarkable influence on S caused by SOC-removed the band degeneracy, and further affects the power factor^{20,21,23,25}. The SOC not only can reduce the power factor, but can also obviously improve one like WX_2 ($X=S, Se$ and Te)²⁰. However, for unstrained MXY ($M = Mo$ or W , $X/Y = S, Se$, or Te) monolayer, only obviously reduced effect can be observed by SOC. The strain-improved S can also found in TMD monolayers, such as MoS_2 , $PtSe_2$, $PtTe_2$, ZrS_2 and $ZrSe_2$ ^{21,23-25,42}, and the related mechanism is similar with that of strain-enhanced S of Janus TMD monolayers. Besides strain, electric field can also effectively tune the electronic structures of 2D materials, so it is possible to tune S of Janus TMD monolayers by electric field. The Janus TMD monolayers may have better thermoelectric properties than TMD monolayers due to lower κ_L . It has been proved that the MoSSe ($ZrSSe$) has lower κ_L than MoS_2 (ZrS_2)^{31,32}, and the $ZrSSe$ has enhanced n-type thermoelectric properties compared with monolayer ZrS_2 ³².

In summary, we systematically study strain depen-

dence of electronic structures and transport coefficients of Janus MXY ($M = \text{Mo or W}$, $X/Y = \text{S, Se, or Te}$) monolayer, based mainly on the reliable first-principle calculations. Calculated results show that the inclusion of SOC is key for energy band structures of Janus TMD monolayers, which has important effects on their electronic transport coefficients. It is found that both compressive and tensile strain can tune the strength of bands convergence by changing the numbers and relative position of VBE or CBE, producing important effects on their electronic transport coefficients. For all Janus TMD monolayers, the S can be enhanced by choosing the appropriate com-

pressive or tensile strain, and then the power factor can be improved. Our works will motivate farther experimental studies, and studies of electronic transports of other Janus TMD monolayers.

ACKNOWLEDGMENTS

This work is supported by the National Natural Science Foundation of China (Grant No. 11404391). We are grateful to the Advanced Analysis and Computation Center of CUMT for the award of CPU hours to accomplish this work.

-
- ¹ Y. Pei, X. Shi, A. LaLonde, H. Wang, L. Chen and G. J. Snyder, *Nature* **473**, 66 (2011).
 - ² A. D. LaLonde, Y. Pei, H. Wang and G. J. Snyder, *Mater. Today* **14**, 526 (2011).
 - ³ M. S. Dresselhaus et al. *Adv. Mater.* **19**, 1043 (2007).
 - ⁴ L. D. Hicks and M. S. Dresselhaus, *Phys. Rev. B* **47**, 12727 (1993).
 - ⁵ L. D. Hicks and M. S. Dresselhaus, *Phys. Rev. B* **47**, 16631(R) (1993).
 - ⁶ K. S. Novoselov et al., *Science* **306**, 666 (2004).
 - ⁷ M. Chhowalla, H. S. Shin, G. Eda, L. J. Li, K. P. Loh and H. Zhang, *Nature Chemistry* **5**, 263 (2013).
 - ⁸ R. X. Fei, W. B. Li, J. Li and L. Yang, *Appl. Phys. Lett.* **107**, 173104 (2015).
 - ⁹ S. L. Zhang M. Q. Xie, F. Y. Li, Z. Yan, Y. F. Li, E. J. Kan, W. Liu, Z. F. Chen, H. B. Zeng, *Angew. Chem.* **128**, 1698 (2016).
 - ¹⁰ J. P. Ji, X. F. Song, J. Z. Liu et al., *Nat. Commun.* **7**, 13352 (2016).
 - ¹¹ S. Balendhran, S. Walia, H. Nili, S. Sriram and M. Bhaskaran, *small* **11**, 640 (2015).
 - ¹² W. Huang, H. X. Da and G. C. Liang, *J. Appl. Phys.* **113**, 104304 (2013).
 - ¹³ G. Qin, Z. Qin, W. Fang, L. Zhang, S. Yue, Q. Yan, M. Hu and G. Su, *Nanoscale* **8**, 11306 (2016).
 - ¹⁴ S. D. Guo and Y. H. Wang, *J. Appl. Phys.* **121**, 034302 (2017).
 - ¹⁵ G. P. Li, G. Q. Ding and G. Y. Gao, *J. Phys.: Condens. Matter* **29**, 015001 (2017).
 - ¹⁶ D. C. Zhang, A. X. Zhang, S. D. Guo and Y. F. Duan, *RSC Adv.* **7**, 24537 (2017).
 - ¹⁷ L. M. Sandonas, D. Teich, R. Gutierrez, T. Lorenz, A. Pecchia, G. Seifert and G. Cuniberti, *J. Phys. Chem. C* **120**, 18841 (2016).
 - ¹⁸ S. D. Guo, A. X. Zhang and H. C. Li, *Nanotechnology* **28**, 445702 (2017).
 - ¹⁹ G. P. Li, K. L. Yao and G. Y. Gao, *Nanotechnology* **29**, 015204 (2018).
 - ²⁰ S. D. Guo and J. L. Wang, *Semicond. Sci. Tech.* **31**, 095011 (2016).
 - ²¹ S. D. Guo and Y. Wang, *Semicond. Sci. Tech.* **32**, 055004 (2017).
 - ²² E. Scalise, M. Houssa, G. Pourtois, V. Afanas'ev and A. Stesmans, *Nano Res.* **5**, 43 (2012).
 - ²³ S. D. Guo, *Comp. Mater. Sci.* **123**, 8 (2016).
 - ²⁴ H. Y. Lv, W. J. Lu, D. F. Shao, H. Y. Lub and Y. P. Sun, *J. Mater. Chem. C* **4**, 4538 (2016).
 - ²⁵ S. D. Guo, *J. Mater. Chem. C* **4**, 9366 (2016).
 - ²⁶ A. Y. Lu, H. Y. Zhu, J. Xiao et al., *Nature Nanotechnology* **12**, 744 (2017).
 - ²⁷ X. C. Ma, X. Wu, H. D. Wang and Y. C. Wang, *J. Mater. Chem. A* **6**, 2295 (2018).
 - ²⁸ L. Dong, J. Lou and V. B. Shenoy, *ACS Nano* **11**, 8242 (2017).
 - ²⁹ W. J. Yin, B. Wen, G. Z. Nie and X. L. Wei and L. M. Liu, *J. Mater. Chem. C* **6**, 1693 (2018).
 - ³⁰ F. P. Li, W. Wei, P. Zhao, B. B. Huang and Y. Dai, *J. Phys. Chem. Lett.* **8**, 5959 (2017).
 - ³¹ S. D. Guo, *Phys. Chem. Chem. Phys.* **20**, 7236 (2018).
 - ³² S. D. Guo, arXiv:1712.09064 (2017).
 - ³³ P. Hohenberg and W. Kohn, *Phys. Rev.* **136**, B864 (1964); W. Kohn and L. J. Sham, *Phys. Rev.* **140**, A1133 (1965).
 - ³⁴ P. Blaha, K. Schwarz, G. K. H. Madsen, D. Kvasnicka and J. Luitz, WIEN2k, an Augmented Plane Wave + Local Orbitals Program for Calculating Crystal Properties (Karlheinz Schwarz Technische Universität Wien, Austria) 2001, ISBN 3-9501031-1-2
 - ³⁵ J. P. Perdew, K. Burke and M. Ernzerhof, *Phys. Rev. Lett.* **77**, 3865 (1996).
 - ³⁶ A. H. MacDonald, W. E. Pickett and D. D. Koelling, *J. Phys. C* **13**, 2675 (1980).
 - ³⁷ D. J. Singh and L. Nordstrom, *Plane Waves, Pseudopotentials and the LAPW Method*, 2nd Edition (Springer, New York, 2006).
 - ³⁸ J. Kunes, P. Novak, R. Schmid, P. Blaha and K. Schwarz, *Phys. Rev. B* **64**, 153102 (2001).
 - ³⁹ D. D. Koelling, B. N. Harmon, *J. Phys. C: Solid State Phys.* **10**, 3107 (1977).
 - ⁴⁰ G. K. H. Madsen and D. J. Singh, *Comput. Phys. Commun.* **175**, 67 (2006).
 - ⁴¹ X. F. Wu, V. Varshney et al., *Chem. Phys. Lett.* **669**, 233 (2017).
 - ⁴² D. Qin, X. J. Ge, G. Q. Ding, G. Y. Gao and J. T. Lv, *RSC Adv.* **7**, 47243 (2017).